Fluid simulation of a microwave plasma cathode

IEPC-2013-396

Presented at the 33rd International Electric Propulsion Conference,
The George Washington University • Washington, D.C. • USA
October 6 – 10, 2013

L. Liard[1,2 †] , Y. Zhu[1,2], G.J.M. Hagelaar[1,2] and J.-P. Boeuf[1,2]
[1]*Université de Toulouse ; UPS, INPT ; LAPLACE (Laboratoire Plasma et Conversion d'Energie) ; 118 route de Narbonne, F-31062 Toulouse cedex 9, France.*

[2]*CNRS ; LAPLACE ; F-31062 Toulouse, France.*

Abstract: The low-temperature plasma of a microwave resonant cavity used as a plasma electron source is described with a semi-analytical model and a fluid simulation. Both models show that the energy cost per electron-ion pair created in the source is around 50 eV in a large pressure range between 20 and 200 mTorr. This corresponds to a value of 20 mA/W of the electron current that can be extracted from the source, consistent with the experimental data in the literature.

Nomenclature

A	=	Total surface of the plasma part in the cavity
A_e	=	aperture surface
α	=	fraction of neutral atoms on the metastable state
D_a	=	ambipolar diffusion coefficient
E_j	=	energy threshold of the reaction j
ϵ_c	=	energy lost by electrons in the volume per electron-ion pair created
ϵ_e	=	energy carried by electrons to the walls
ϵ_i	=	energy carried by ions to the walls
ϵ_T	=	total energy loss per electron-ion pair created
ε_r	=	relative electrical permittivity
Λ	=	diffusion length of the plasma
η_i	=	fraction of the metastable states contribution to the overall ionization
I_e	=	total electron current to the walls
I_i	=	total ion current to the walls
J_j	=	Bessel function of the j^{th} order
k_B	=	Boltzmann constant
K_j	=	constant rate of the reaction j
L	=	length of the plasma part of the cavity
L_c	=	energy loss per electron per unit time by electrons due to collisions in the discharge volume
M	=	xenon atom mass
m_e	=	electron mass
n_0	=	electron density at the center of the plasma
n_e	=	electron density
n_g	=	xenon atoms density
n_m	=	metastable atoms density

[†] Electronic mail : laurent.liard@laplace.univ-tlse.fr

n_s = electron density at the sheath edge
$\bar{n}$ = mean electron density
ν_I = total ionization frequency for electrons
P_{abs} = total absorbed power in the plasma
P_{loss} = power lost by charged particles
Q_0 = flow rate of gas inlet
r = radial direction
R = radius of the cavity
T_e = electron temperature
u_B = Bohm velocity
V = Total volume of the plasma part of the cavity
x = axial direction
χ_{ij} = j^{th} zero of the i^{th} Bessel function order

I. Introduction

Neutralization of the ion beam of an electric thruster is an important aspect of electric propulsion. Hollow cathodes[1] are commonly used as electron sources to provide the needed electron current. They can be made of different materials with low work function. When heated at a sufficiently high temperature, the material surface emits electrons that ionize the gas injected through the cathode. The electron current is extracted through an orifice in the discharge chamber, by an externally applied voltage. Although hollow cathodes exhibit impressive characteristics for current emission and power consumption, their making remains complex and expensive and their sensitivity to oxygen contamination can be prohibitive for some specific missions (very low orbit missions for example).

For these reasons, research on alternative plasma cathode electron sources that do not contain any thermo-electronic material is still active[2]. Several plasma cathode designs have been characterized, mostly based on microwave and radiofrequency excitation: Godyak *et al.*[3] presented a ferromagnetic ICP (Inductively Coupled Plasma) excited at 2 MHz, which exhibits an extracted current of 25 mA/W in xenon gas in a large range of plasma and input power. Nakabayashi *et al.*[4] also proposed an ICP radiofrequency plasma excitation at 13.56 MHz, with an efficiency close to 20 mA/W. Microwave excitation in a 5.8 GHz resonant cavity has also been investigated by Diamant[5-6]. In a first set of experiments[5], the cavity was able to deliver around 30 mA/W with xenon without magnetic field. A strong axial magnetic field generated by permanent magnets was then added[6], leading to an enhanced the efficiency of the cathode of 90 mA/W for Xenon and 50 mA/W for argon. Weatherford and Foster[7-8] also proposed a magnetized microwave plasma, excited by Electron Cyclotron Resonance, and obtained an efficiency of 11 mA/W, with losses to the electron current probe included in the calculation.

In this paper, we present a global analytical and a fluid numerical model of the low-temperature plasma generated by a microwave source in the same range of pressure and input power as Diamant's microwave resonant cavity[5-6]. The simulated electron source and the principles of the models are described in section II. The details of the global 0D model (based on global particle and energy balance in the plasma source) and the results are given in section III. Section IV presents the results of the more complex 2D fluid simulations, which include gas heating and refine the 0D model results. Section V presented the conclusion of this work.

II. Simulated source and principles of the models

In this section, the simulated plasma source and the principles of the models are described.

A. Microwave plasma source

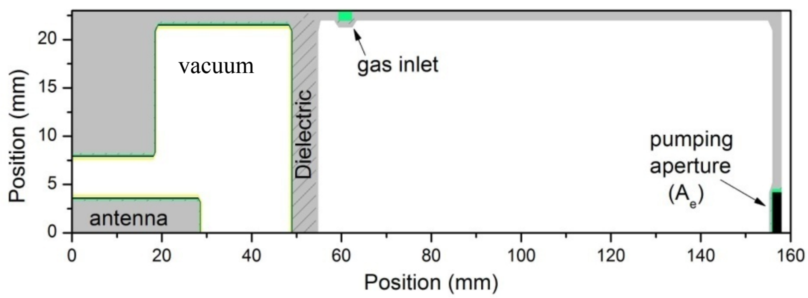

Figure 1. Sketch of the 2D simulation domain of the cylindrical microwave resonant cavity. Only the upper part of the cavity is drawn. Microwaves are injected on the left part, through the coaxial cable.

Figure 1 presents a sketch of the calculation domain used to model the resonant cavity. Only a section of the cylindrical cavity is drawn, as the source is symmetrical around its axis. Microwaves are injected on the left side, through a coaxial cable of 50 **Ω**, which is partially drawn. The core of the coaxial cable is inserted 9 mm into the cavity, and acts as a microwave antenna. On the left side of the dielectric, the material is vacuum, so its electric permittivity is set to 1, and no plasma can be triggered in this domain. The injection region (vacuum) is separated from the plasma by a dielectric window. The dielectric material is set with a thickness of 4 mm and an electric permittivity corresponding to alumina (ϵ_r=9.6). This dielectric window prevents the microwave antenna from being in contact with the plasma. On the right part of the dielectric, where the plasma is ignited, neutral atoms are injected from a gas inlet located on the side of the cylinder with a specified flow rate Q_0 [s^{-1}] and pumped through an aperture with a surface A_e in the exit plane. All the metallic parts are assumed to be perfectly conducting.
The dimensions of this metallic cavity have been chosen to excite the mode TM_{011} at a 5.8 GHz microwave frequency, and to optimize plasma breakdown at this frequency. If analytical formula are available to design homogeneous cavity, the presence of an antenna and the dielectric window makes it non homogeneous. Consequently, the cavity dimensions that are required to get the desired mode at the microwave frequency must be obtained numerically. In the simulation, the chamber radius is 20 mm and the total length of the cavity is composed by 100 mm of plasma part, 5 mm of dielectric and 28 mm of vacuum part.

B. Principles of the models

As mentioned above, two different models have been used to characterize the source: a 0D model, based on global particle and energy balance in the chamber, and a 2D fluid model able to provide the space and time variations of the plasma properties. The principles of the 2D fluid model (CAVIMO) are described in details in the paper by G.J.M. Hagelaar[9]. The model is based on the self-consistent description of the coupling between Maxwell's equations and the plasma fluid equations. Nevertheless, preliminary simulations have shown that the microwave power, injected through the dielectric window is absorbed in a thin skin depth next to the dielectric surface and that the simulation results do not strongly depend on the thickness of this layer. Therefore, in order to minimize the numerical burden, all the plasma simulations presented here have been performed by assuming that the power is uniformly absorbed in a layer of 2 mm thickness next to the dielectric window.

C. Xenon kinetic scheme

This section presents the gas scheme used for the xenon gas in the simulation. Sommerer[10] has developed a complete model for xenon, in the same range of pressure. The electron-neutral cross-section used in this paper have been taken from the LXCAT website[11] (same cross-section as in Meunier *et al.*[12]). The constant rates are calculated assuming a Maxwellian electron distribution function. Indeed, because of the rather important ionization degree in the cavity (1% or more) electron-electron Coulomb collisions play an important role and lead to a Maxwellian electron distribution function. Table 1 presents the reactions included in the xenon chemistry model. The simplicity of the model allows solving analytically the particle balance, and therefore discussing precisely the contribution of every term. A level of metastable atoms has been considered, which results into two different mechanisms to create electrons: direct and stepwise ionization. Superelastic collisions and stepwise ionization are the only processes destroying metastable atoms.

Reaction	Type	Rate ($m^3 s^{-1}$)
$e^- + Xe \rightarrow e^- + Xe$	elastic	K_{el}
$e^- + Xe \rightarrow e^- + Xe*$	Metastable excitation	K_{ex}
$e^- + Xe* \rightarrow 2e^- + Xe^+$	Stepwise ionization	K_{sw}
$e^- + Xe* \rightarrow e^- + Xe$	Metastable de-excitation	K_{de}
$e^- + Xe \rightarrow 2e^- + Xe^+$	Ionization	K_{iz}

Table 1. Reactions included in the xenon chemistry model for 0D and 2D models.

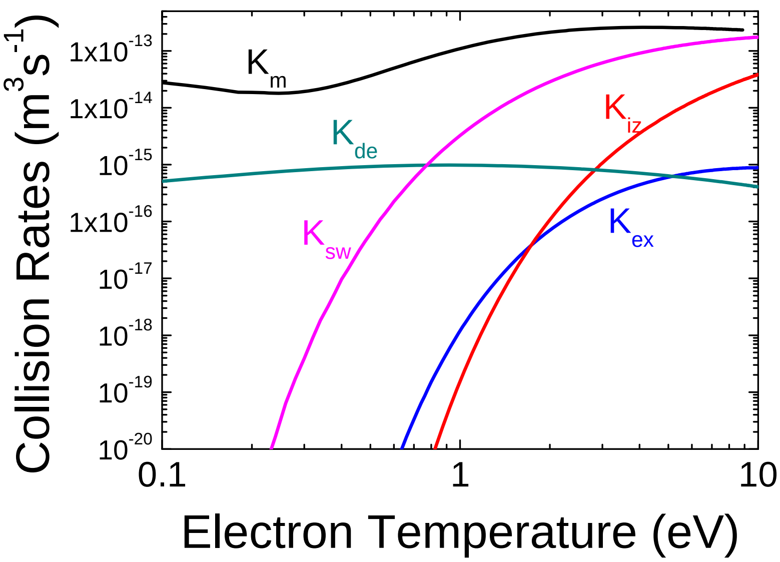

Figure 2. Rate coefficients as a function of electron temperature for the reactions of Table 1, calculated from the cross-section data of Meunier[12], assuming a Maxwellian electron distribution function.

III. Global model description and results

A. Particle balance equation

To get a first order description of the plasma and form the basis to understand and discuss the results from the more complex 2D model, a global 0D model based on global equations is presented[13]. Particle balance equation relates the ionization rate integrated over the discharge volume, to the charged particle losses (Bohm flux) at the surfaces integrated over the chamber walls, and fixed the electronic temperature T_e. The power balance relates the power absorbed by electrons in the plasma to the power dissipated by charged particles through collisions in the volume, and carried to the walls and fixes the average plasma density $\bar{n}$. This model does not describe the details of the transport of particles and energy in the discharge volume but takes into account the particles and energy transported to the walls.

The model presented here is based on a pressure range where the ion mean free path is much smaller than the discharge dimensions, which appears to be the case for experimental resonant microwave plasma cathodes. In this case, the charged particles fluxes are ambipolar and the steady state diffusion equation has the form of Poisson's equation, where the right term correspond the volume creation of charged particles.

(1) $$-D_a \nabla^2 n = \nu_I n$$

where D_a is the ambipolar diffusion coefficient and ν_I the total ionization frequency. The assumption of a uniform electron temperature makes these coefficients independent of the electron density. Solving this equation in a cylinder of radius R et length L, the electron density can be expressed as :

(2) $$n(x,r) = n_0 J_0(\chi_{01} r/R) \cos(\pi x/L)$$

The plasma density profile is defined as the product of a cosine profile along the axial direction x, times a Bessel J_0 profile in the radial direction r. $\chi_{01} \approx 2.405$ is the first zero of the Bessel function J_0. The continuity equation above is an eigenvalue equation and the conditions of zero density at the wall surface require that:

(3) $$\frac{\nu_I}{D_a} = \left(\frac{\chi_{01}}{R}\right)^2 + \left(\frac{\pi}{L}\right)^2 = \left(\frac{1}{\Lambda}\right)^2$$

Let's now detail the source term ν_I for electrons: they are created in the volume either by direct or stepwise ionization, and are lost only to the surface.

(4) $$\nu_I n = n n_g K_{iz} + n n_m K_{sw}$$

where n_m and n_g are respectively the metastable density and the ground state xenon atoms density. The direct ionization rate K_{iz} and the stepwise ionization rate K_{sw} are constant as the electron temperature is assumed uniform in this model. This assumption is confirmed in the next section.

The metastable density n_m can be obtained from a balance equation for the metastable atoms: these atoms are produced by excitation of the xenon atoms and destroyed by electron impact de-excitation or stepwise ionization. Assuming that the losses to the walls are small with respect to the volume creation and losses (this is confirmed by the fluid simulation), balance of production and losses at steady state gives:

(5) $$n_e n_g K_{ex} = n_e n_m K_{sw} + n_e n_m K_{de}$$

Therefore, the metastable density is proportional to the gas density:

(6) $$n_m = \frac{K_{ex}}{K_{sw} + K_{de}} n_g = \alpha n_g$$

where $\alpha = K_{ex}/K_{sw} + K_{de}$ represents the fraction of neutral atoms on the metastable state and is only a function of the electron temperature T_e. The total volume creation of electrons can then be expressed as:

(7) $$\nu_I = n_g(K_{iz} + \alpha K_{sw})$$

In our conditions, the electron temperature is much larger than the ion temperature and the ambipolar diffusion coefficient becomes:

(8) $$D_a \approx \frac{k_B T_e}{M n_g K_{in}}$$

where k_B is the Boltzmann constant, M the ion xenon mass, $K_{in} \approx 5.3\ 10^{-16}$ m^3.s^{-1} the ion-neutral collision constant rate[14]. Finally, the equation that fixes the electron temperature in our plasma cylinder can be written as:

(9) $$K_{iz} + \alpha K_{sw} = \frac{k_B T_e}{M K_{in}} \left(\frac{1}{n_g \Lambda} \right)^2$$

The left hand side of this equation depends only on electron temperature, while the right hand side depends on the gas density and discharge dimension. This means that the electron temperature is completely determined by the gas density and discharge dimensions and does not depend on the power absorbed in the discharge, for a fixed gas density.

Equation (is solved for different values of gas density or pressure and for the considered discharge geometry, using the rate coefficients as a function of electron temperature given in the previous section. The calculated electron temperature as a function of gas pressure is displayed in Fig. 3. On this figure is also represented the fractional contribution of the metastable states to the overall ionization, defined as:

(10) $$\eta_i = \frac{n_m K_{sw}}{n_m K_{sw} + n_g K_{iz}} = \frac{\alpha K_{sw}}{\alpha K_{sw} + K_{iz}}$$

Figure presents an electron temperature around 1 eV that decreases from about 1.5 eV at 0.02 Torr to 0.8 eV at 0.2 Torr. These variations look relatively small for a variation of a factor of 10 of the pressure and gas density. However, Fig. 2 stresses that a relatively small variation in electron temperature is actually associated with a very large variation of the charged particle volume production frequency and losses to the walls. The contribution η_i of the metastable states to the overall ionization through stepwise ionization is quite large, between 60% and 90% over the range of pressure considered and is smaller at lower pressure, as expected since second kind collisions are less important at lower pressures. The electron temperature when the contribution of metastable to ionization is not included in the calculations is also shown for comparisons in Figure . We see that the electron temperature must be larger by about 0.2 eV for the discharge to be sustained when stepwise ionization is not included. However, the following section shows that the plasma density is considerably reduced without metastable ionization.

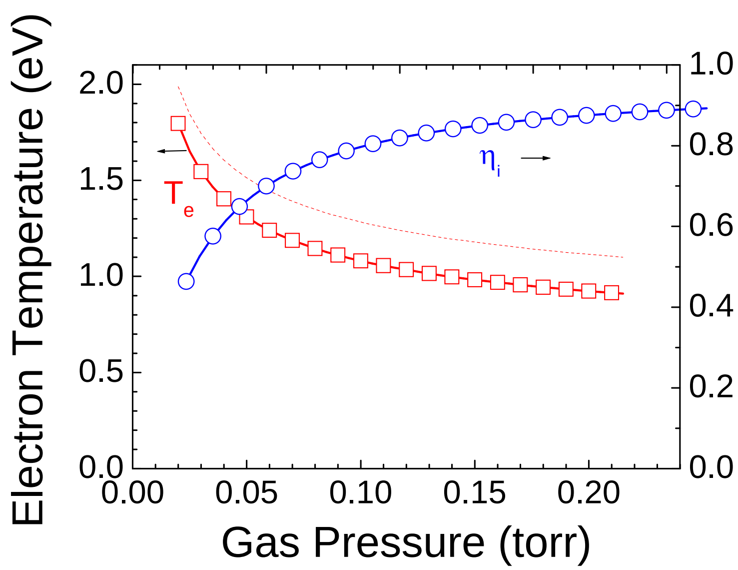

Figure 3. Electron temperature T_e and fractional contribution of metastable atoms to the overall ionization η_i, as a function of gas pressure, from the global model. The dashed line corresponds to a case where stepwise ionization of the metastable atoms is not considered.

B. Power balance equation

The plasma density in a global model can be obtained from a simple expression of the power balance in the discharge. The power absorbed in the discharge by electrons must be balanced by the losses through collisions in the volume plus the energy losses to the walls. At low pressure, the losses to the walls can be quite large whereas at higher pressure, the energy losses in the volume are dominant.
Before writing the power balance equation, this global model of collisional plasma contains a non-uniform plasma density distribution as defined in equation (2). The average plasma density $\bar{n}$ is analytically related to the maximum density through:

(11) $$\bar{n} = \frac{4J_1(\chi_{01})}{\pi\chi_{01}} n_0 \approx 0.28\, n_0$$

where J_1 is the Bessel function of first order. Let us now write that the power absorbed by the electrons is equal to the sum of the power lost in the volume and on the surface of the chamber:

(12) $$P_{\mathrm{abs}} = P_{\mathrm{loss}} = \bar{n}VL_c + n_s u_B A(\epsilon_e + \epsilon_i)$$

where P_{abs} is the total power absorbed (by electrons) in the discharge, and P_{loss} is the power lost by charged particles, which is composed of volume power losses $\bar{n}VL_c$ and surface power losses $n_s u_B A(\epsilon_e + \epsilon_i)$. The surface power losses is obtained by multiplying the flux of particles (electron and ions) to the walls integrated over the surface, $n_s u_B A$, by the sum of the energy carried by electrons and ions to the walls, respectively ϵ_e and ϵ_i. In the volume loss term, L_c is the energy loss per electron per unit time by electrons due to collisions in the discharge volume. By introducing the energy lost by electrons in the volume per electron-ion pair created $\epsilon_c = L_c / \upsilon_I$, and using equation (), the averaged plasma density is extracted from the power balance equation above, to give:

(13) $$\bar{n} = \frac{P_{\mathrm{abs}}}{V}\frac{M}{k_B T_e}\frac{K_{in} n_g \Lambda^2}{\epsilon_T}$$

where $\epsilon_T = \epsilon_c + \epsilon_e + \epsilon_i$ is the total energy loss per electro-ion pair to the walls. The detailed calculation of these different energy loss terms for a Maxwellian distribution function is well described in Lieberman[13]: energy carried by electrons in one direction is classically given by $\epsilon_e = 2k_B T_e$ and ion energy carried to the walls is the sum of the energy gained in the sheath and the ion energy at the sheath entrance.

(14) $$\epsilon_i = \frac{k_B T_e}{2}\left[1 + \ln\left(\frac{M}{2\pi m_e}\right)\right]$$

Note that this ion energy loss corresponds to the energy transported to the walls and does not include the energy deposited by ions through collisions in the gas. These losses can lead to gas heating. It is difficult to get an exact analytical expression for the losses by ions in the volume (Joule heating). In order to keep the global model simple, these losses are neglected in this model and their influence will be checked in the complete 2D simulations. Therefore, only electron energy losses are considered. The energy lost per electron per unit time, as written in the electron energy equation is:

(15) $$L_c = n_g K_{el} T_e \frac{3m_e}{M} + n_g \sum_j K_j E_j + n_g K_{iz} E_{iz} + n_m E_{sw} K_{sw} - n_m E_{de} K_{de}$$

This expression accounts for electron losses due to elastic collisions (first term), total electronic excitation (second term), direct ionization (third term), stepwise ionization (fourth term), and de-excitation (last term). The energy loss rates for elastic collision, total excitation, and ionization, respectively $K_{el} T_e \frac{3m_e}{M}$, $\sum_j K_j E_j$, and $K_{iz} E_{iz}$ are plotted as a function of electron temperature in Fig. 4. The energy loss rates for stepwise ionization and de-excitation can be deduced by multiplying the rate coefficients K_{sw} and K_{de} of Tab. 1 by their corresponding energy threshold (respectively 3.44 and 8.31 eV).

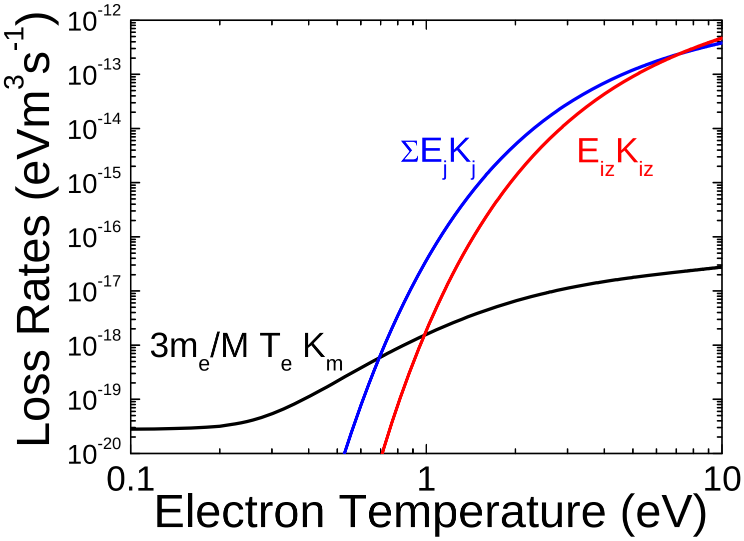

Figure 4. Electron energy loss rate coefficients corresponding to elastic collisions (black line), total electronic excitation (blue), and ionization (red) as a function of electron temperature, calculated from the cross-section data assuming a Maxwellian electron distribution function. The energy loss coefficient for stepwise ionization and de-excitation (energy gain) can be simply deduced from the corresponding rates of Fig. 2.

From eq. (7), the expression of ϵ_c appears:

(16)
$$\epsilon_c = \frac{K_{el} T_e \frac{3m_e}{M} + \sum_j K_j E_j + K_{iz} E_{iz} + \alpha(E_{sw} K_{sw} - E_{de} K_{de})}{K_{iz} + \alpha K_{sw}}$$

Equation (13) shows that for a given gas density, since the electron temperature is independent of the absorbed power, the plasma density varies linearly with absorbed power. Figure displays the variations of the plasma density obtained with this expression, as a function of gas pressure and for different values of the absorbed power, from 10 to 60 W. This figure confirms the linear increase of the plasma density with power at constant gas density, and shows, as expected an increase of the plasma density with increasing pressure for a given absorbed power.

The results displayed in Fig. 6 show that under our conditions the energy lost to the wall per electron-ion pair created, ϵ_c does not vary strongly with gas pressure and is on the order of 40 eV. Since ϵ_e and ϵ_i depend only on electron temperature which does not present very large variations in the considered pressure range, we can deduce that the total energy lost per electron-ion pair to the wall, $\epsilon_T = \epsilon_c + \epsilon_e + \epsilon_i$ does not depend strongly on pressure.
It appears on Fig. 5 that the plasma density for a given power increases almost linearly with pressure or gas density. This can be understood by looking at the expression of the plasma density, eq. (13). Its denominator depends only slightly on gas pressure since it contains only ϵ_T and $T_e$which are slow functions of the gas pressure in our pressure range. The numerator is proportional to the ion collision frequency and therefore to the gas density or gas pressure. The absorbed power therefore behaves almost as a linear function of the gas density or gas pressure. The total energy loss per electron-ion pair (Figure) to the wall is a very important parameter since it determines the discharge efficiency. When designing an electron source, the energy cost per electron extracted must be minimized. In this source, the minimum energy cost per extracted electron is therefore equal to ϵ_T, and is on the order of 50 eV.

Another way to discuss the efficiency of this source consists in quantifying the maximum current of electron that can be extracted. This maximum current is equal to the total electron current to the walls. For a power of 60 W, the maximum electron current that can be extracted is e*P*/*E*$_c$ i.e. is on the order of 1.2 A in our conditions.

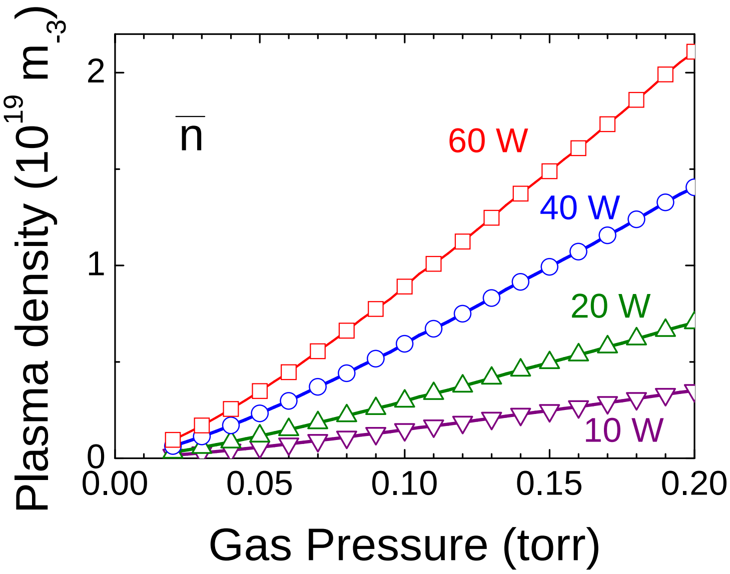

Figure 5. Averaged plasma density as a function of gas pressure and for different absorbed power, from the 0D model. Equation (11) specifies that the maximum plasma density is about 3.5 larger than the averaged plasma density.

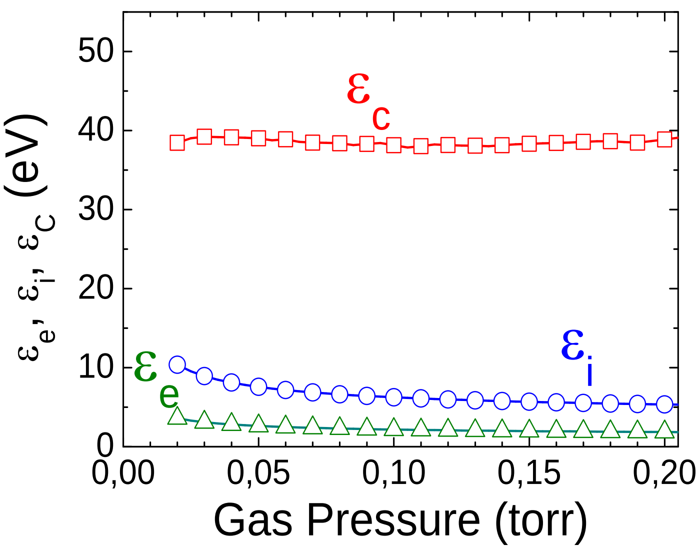

Figure 6. Electron and ion energy losses to the walls, ϵ_e ϵ_i, and electron energy loss per electron-ion pair to the wall, ϵ_c as a function of electron temperature as described in eqs. (14) and (16).

This is confirmed in Figure which displays the electron and ion current to the walls as a function of gas pressure and for different values of the power absorbed in the discharge. The current in this figure are deduced from the previous equations:

(17) $$I_e = I_i = en_s \mathrm{u}_B A = e\bar{n}Vn_g(K_{iz} + \alpha K_{sw}) = \frac{eP_{\text{abs}}}{\epsilon_T}$$

Note that equation **Error! Reference source not found.**) and Figure give the maximum extracted electron current, i.e. assuming that all the electrons are extracted using an extraction system with a proper extraction voltage. The question of electron extraction from the source is treated in the next section.

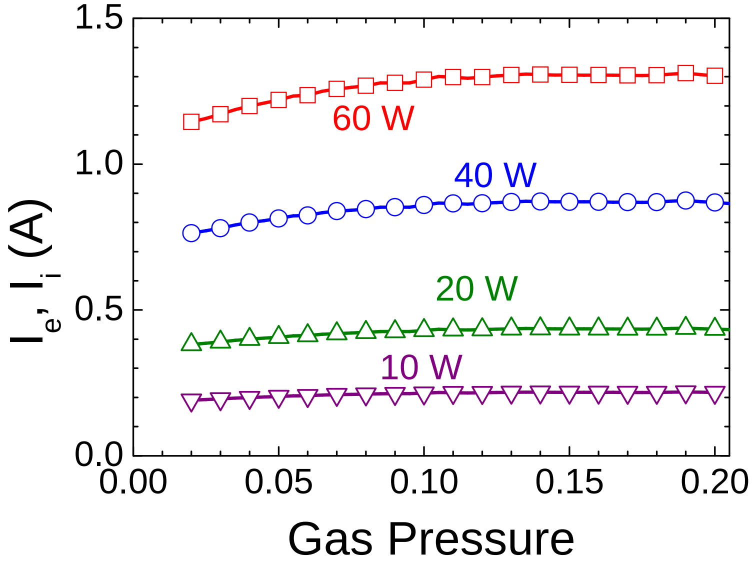

Figure 7. Total electron and ion currents to the wall as a function of gas pressure and for different values of the absorbed power.

Finally, the global fluid model has given an overall description of the plasma inside the cavity : the pressure and the metastable state cause the electronic temperature to remain near 1 eV near 100 mTorr. The mean electron density reaches 1 10^{19} m^{-3} at 100 mTorr and 60 W of input power. However, the main limitation to create a dense plasma is the total energy loss per pair electron-ion created ϵ_T. Its value remains at 50 eV and does not depend strongly on the pressure range.

IV. 2D fluid simulation of the plasma: a finer picture

This section presents a 2D fluid simulation of the plasma part of the cavity, with 60W absorbed power. This power is absorbed on a 2 mm skin depth next to the dielectric. In Diamant's experiment, the flow rate is on the order Q_0=1 mg.s^{-1} (10.25 sccm). Keeping the same flow and the same pumping aperture as the experiment, $A_e = 5\ 10^{-5}$ m^2, the Clausing factor[15] is adjusted to keep a 100 mTorr pressure inside. Results presented here consider the plasma without gas heating in part A, and then with gas heating in part B.

A. Plasma simulation without gas heating

Figure 8 displays the spatial variations of the main parameters of the plasma inside the cavity. On Fig. 8a), the electron density exhibits a maximum value of 2.8 10^{19} m^{-3} on the discharge axis at about 20 mm from the dielectric surface. From this maximum, the plasma density decreases by a factor of about 10 over 8 cm along the discharge axis. This relatively fast decrease is consistent with ambipolar diffusion in this collisional regime. Note also that the calculated plasma density in the 2D model is in remarkably good agreement with the estimation of the global 0D model of the previous section, where the plasma density was about 2 10^{19} m^{-3} and the metastable density was around 0.8 10^{18} m^{-3} for the same pressure and input power. The difference between the 2D and 0D models are mainly due to the fact that the absorbed power is located in a thin layer next to the dielectric wall. This creates a (small) non-uniformity in the electron temperature (slightly larger next to the dielectric wall, see **Error! Reference source not found.**b).

Since the rates are very non-linear functions of the electron temperature, this leads to significantly larger non-uniformities of the metastable density and plasma density (which are larger next to the dielectric wall). The 0D model cannot describe these transport effects. Note that for this reason, we can expect larger differences between the 0D and 2D model when the pressure increases (smaller thermal diffusion of the electrons).

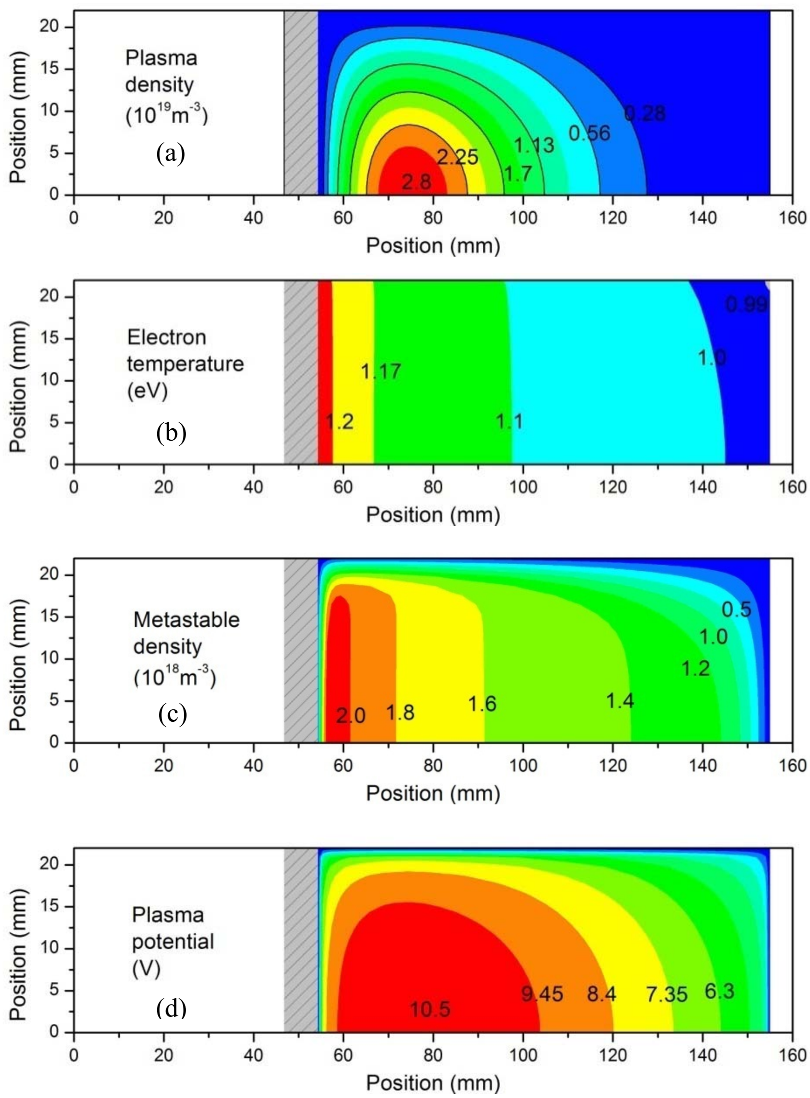

Figure 8. 2D distribution of the plasma properties obtained assuming a fixed gas density at 100 mTorr, with an input power of 60 W. a) plasma density, b) electron temperature, c) metastable density, d) plasma potential.

The electron temperature in the cavity displayed in Fig. 8b) shows small spatial variations between 0.99 and 1.2 eV (mainly in the axial direction), again in agreement with the 0D model where the electron temperature was about 1 eV under these conditions. As said above, the electron temperature rises near the dielectric window since the power is supposed to be absorbed in this region.

The metastable density distribution of Fig. 8c) presents a maximum value of 2 10^{18} m^{-3} in the vicinity of the dielectric surface. The metastable density decreases mostly axially, following electron temperature variations. Indeed, the production rate of the metastable is a fast increasing function of the electron temperature around 1 eV (see Fig. 2) and although the variations of electronic temperature are not very important, the associated variations of the metastable production are relatively large, which explains the larger metastable density near the dielectric surface where the electron temperature is larger. Also, the reactions involving the metastable atoms are dominant over transport due to diffusion, and this explains the maximum close to the dielectric surface. It is interesting to note that in our simple chemistry model and if the transport terms in the metastable transport equation are not important, the metastable density is simply given by eq. **Error! Reference source not found.**) of the 0D model. This equation shows that the metastable density depends only on the electron temperature through constant rates and is proportional to the gas density. Indeed, figure 8 shows that the metastable density distribution follows the electron temperature distribution, with amplification due to the fact that the rates of production and destruction of the metastable state are very non-linear functions of the electron temperature.

The plasma potential in the cavity, displayed in Fig. 8d), has a maximum of about 10.5 V in the region of maximum plasma density. In spite of the fact that the model does not resolve the sheath, it provides a good estimation of the plasma potential (because the balance of charged particles fluxes is well described in the model) and of the space variations of the plasma properties in the quasi-neutral plasma (the description of charged particle transport in the quasi-neutral plasma does not require to resolve the electron Debye length).

The particle balance integrated on the plasma volume for each species also confirmed the trends observed in the previous section: 78% of the ions and electrons are generated from stepwise ionization, and 22% from direct ionization. These numbers show the importance of taking account of the metastable particles in the calculation.

B. Plasma simulation with gas heating

The effect of gas heating is strongly dependent on boundary conditions, i.e. on the cooling or not of the chamber walls. . We assumed that all metallic walls are cooled to 300 K whereas the dielectric window is not cooled. Figure 9 presents the spatial variations of the main plasma parameters for the same input parameters as Fig. 8, but with gas heating included.

One of the main differences between Fig. 8 and Fig. 9 is the appearance of neutral depletion. Since the neutral gas is heated, the neutral density of xenon atoms decreases to keep a uniform neutral pressure. Quantitatively, the gas reaches 600 K at the vicinity of the dielectric on Fig. 9a), so the gas density is reduced by about 50% at the location of maximum gas temperature on Fig. 9b). Consequently, the plasma density maximum plot on Fig. 9c) is about twice smaller than in the case without gas heating. The overall neutral density decreases, so a higher electronic temperature in Fig. 9d) is required to maintain the plasma and balance higher losses to the wall. Note that the electron temperature increase, although relatively small, leads to an increase in the energy losses to the walls and in the volume. The metastable density on Fig. 9e) is not only following the electronic temperature profile, but also the neutral density profile. Where the neutral density is lower, the metastable density tends also to decrease. The plasma potential profile shown in Fig. 9f) remain almost identical to the previous section.

Finally, the numerical simulation gives the total electron current to the walls, as plotted on Fig. 10. As mentioned in the previous section, these currents give an upper limit of the electron current that can be extracted when the source is used as an electron source. Results obtained by the global model and with the simulation are in good agreement.

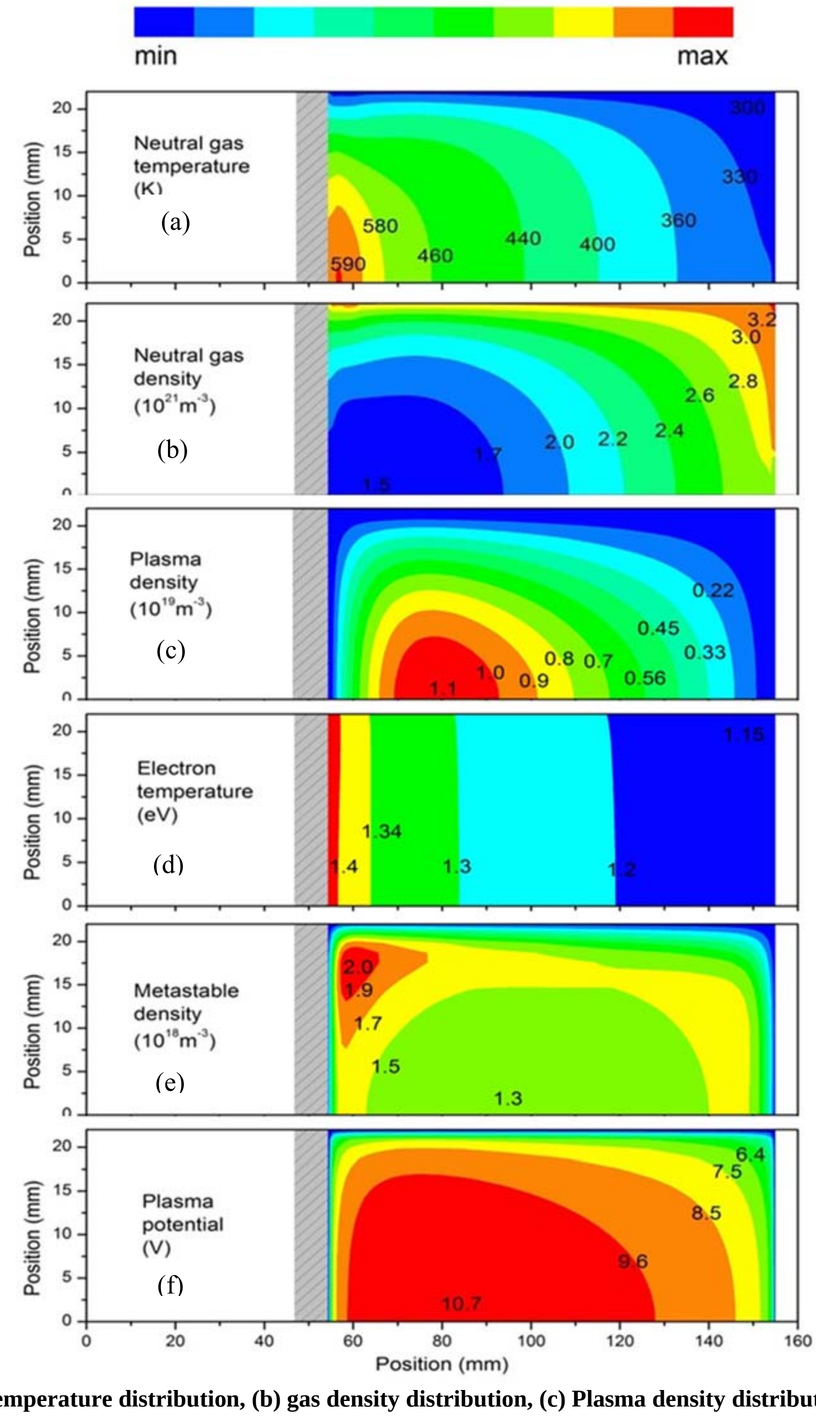

Figure 9. (a) gas temperature distribution, (b) gas density distribution, (c) Plasma density distribution, (d) electron temperature distribution, (e) Metastable density distribution, (f) plasma potential distribution, from the 2D model with fixed injection flow rate.

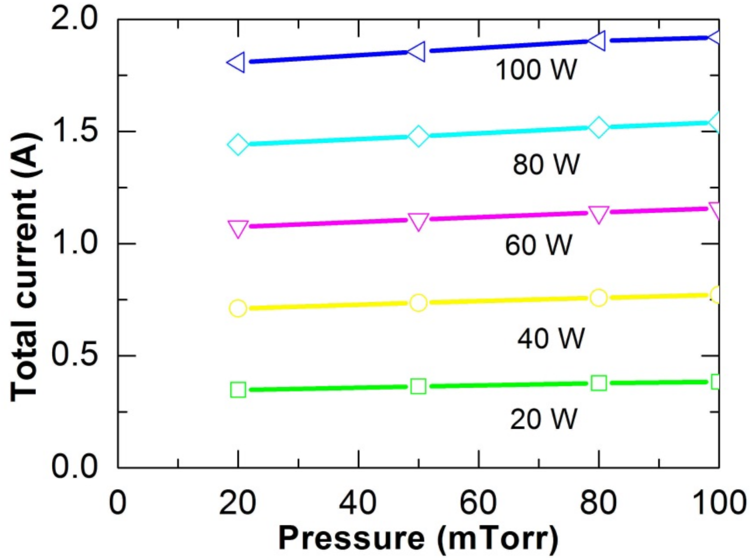

Figure 10. Total electron current to the walls as a function of pressure and for different values of the applied power, from the 2D model with gas heating.

V. Conclusion

We have presented an analytical global model and a 2D numerical fluid model of a low temperature xenon plasma potentially used as a cathode for space propulsion. These models were designed in the range of pressure between 20 and 200 mtorr and input power (60 W) that are typical of plasma electron sources. The global model results exhibit moderate electron temperature, due to the range of pressure and metastable xenon state, and density in the order of 10^{13} cm^{-3}. The analytical study shows that the plasma efficiency to produce high current with moderate input power is limited by ε_T the total energy lost per electron-ion created, whose value is around 50 eV and remains quite uniform over the considered range of pressure. Consequently, the maximum current available in this kind of plasma source, whatever the excitation, is found to be 20 mA/W. This value is similar to experimental data in the literature on plasma cathode using collisional heating without magnetic field. The fluid model confirms and provides more accurate and more detailed results. The upper limit of 20 mA/W deduced from the models corresponds to the maximum current that can be extracted. In practice, part of the electron current must flow to the dielectric surface to balance the ion current to this surface. The simulations (not discussed here) show that 90% of the produced current can be extracted if appropriate extracting conditions are used (voltage and dimensions of the extraction hole).

Finally an important aspect not discussed here is the efficiency of the power coupling from the power supply to the plasma electrons. The ferromagnetic ICP proposed by Godyak[3] for instance achieves 97% power transfert efficiency.

References

[1]Goebel, D., and Katz, I., *Fundamentals of Electric Propulsion: Ion and Hall Thrusters*, John Wiley & sons, New York, 2008, Chap. 6.

[2]Oks, E., *Plasma Cathode Electron Source*, Wiley-vch, Weinheim, Germany, 2006.

[3]Godyak, V., Raitses, Y., and Fisch, N. J., "RF Plasma Cathode-Neutralizer for Space Applications" *Proc. 30th International Electric Propulsion Conference,* Sept. 2007, Paper No. IEPC-2007-266.

[4]Nakabayashi T. *et al*., C. M., "Parametric Study on Shape Dependence of Inductively Coupled Plasma Cathode for Performance Improvement," *Proc. 32nd International Electric Propulsion Conference*, Sept 2011, No. IEPC-2011-305

[5]Diamant, K.D., "Resonant Cavity Plasma Electron Source", *IEEE Transactions on Plasma Science*, Vol. 37, No. 8, 2009, pp. 1558-1562.

[6]Diamant, K. D., "Microwave Cathode for Air Breathing Electric Propulsion", *Proc. 31st International Electric Propulsion Conference*, Sept 2009, No. IEPC-2009-015.

[7]Weatherford, B., Foster, J., and Kamhawi, H., "Improved Performance of the ECR Waveguide Plasma Cathode with Permanent Magnets", *46th AIAA/ASME/SAE/ASEE Joint Propulsion Conference and Exhibit,* AIAA-2010-6519

[8]Weatherford, B., Foster, J., and Kamhawi H. "Electron current extraction from a permanent magnet waveguide plasma cathode. *Rev. Sci. Instrum.*, Vol. 82, No. 9, 2011, p 093507.

[9]Hagelaar, G. J. M., Makasheva, K., Garrigues, L. and Boeuf, J.-P. "Modelling of a dipolar microwave plasma sustained by electron cyclotron resonance", *J. Phys. D: Appl. Phys.*, Vol. 42, 2009, p. 194019.

[10]Sommerer, J.S., "Model of a weakly ionized, low-pressure xenon dc positive column discharge plasma", *J. Phys. D: Appl. Phys.*, Vol. 29, 1996, pp. 769-778.

[11]SIGLO database, http://www.lxcat.laplace.univ-tlse.fr, retrieved July 10, 2013.

[12]Meunier, J., Belenguer, Ph., and Boeuf, J.-P., "extrapolation of allowed cross sections to 1 kV using log(energy)/energy scaling", *J. Appl. Phys.*, Vol. 78, 1995, p. 731.

[13]Lieberman, M. A. and Lichtenberg, A. J., *Principles of plasma discharges and materials processing*, Second Edition, John Wiley & Sons , New York, 2005.

[14]Viehland, L. A. and Mason, E. A., "Transport Properties of Gaseous ions over a wide energy range, IV", Atomic Data and Nuclear Data Tables, Vol. 60, No. 1, 1995, p. 37.

[15]Clausing, P., "The flow of high rarefied gases through tubes of arbitrary length", *Journal of Vacuum Science and Technology*, Vol. 8, No. 5, 1971, pp. 636-646.

[16]Longmier, B. and Hershkowitz, N. "Global nonambipolar flow: Plasma confinement where all electrons are lost to one boundary and all positive ions to another boundary", *Physics of Plasmas*, Vol. 14, No. 4, 2007, p. 042109.